Journal of Power Sources 240 (2013) 494–502

Contents lists available at SciVerse ScienceDirect

Journal of Power Sources

journal homepage: www.elsevier.com/locate/jpowsour

Effect of carbon nanotube diameter for the synthesis of Fe/N/multiwall carbon nanotubes and repercussions for the oxygen reduction reaction

F.J. Pérez-Alonso [a], M. Abdel Salam [b,**], T. Herranz [a], J.L. Gómez de la Fuente [a], S.A. Al-Thabaiti [b], S.N. Basahel [b], M.A. Peña [a], J.L.G. Fierro [a], S. Rojas [a,*]

[a] Grupo de Energía y Química Sostenibles (EQS), Instituto de Catálisis y Petroleoquímica, CSIC, C/Marie Curie, 2, L10. 28049 Madrid, Spain
[b] Chemistry Department, Faculty of Science, King Abdulaziz University, P.O. Box 80200, Jeddah 21589, Saudi Arabia

HIGHLIGHTS

- Fe/N centres have been created onto chemically treated MWCNT with different mean diameters.
- The amount of N incorporated onto the MWCNT increases with their mean diameter.
- Fe/N/CNTS are very active electrocatalysts for the ORR in acid medium.
- N-sites located at the external surface area are the most actives for the ORR.

GRAPHICAL ABSTRACT

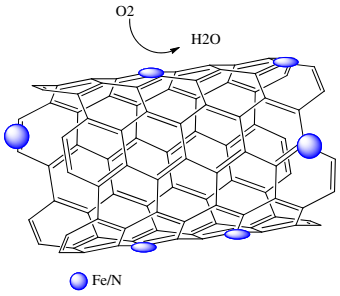

ARTICLE INFO

Article history:
Received 19 January 2013
Received in revised form
13 April 2013
Accepted 17 April 2013
Available online 26 April 2013

Keywords:
Pt-free
Oxygen reduction reaction
Multiwalled carbon nanotubes
Fe
N

ABSTRACT

The effect of the diameter of multiwalled carbon nanotubes for the incorporation of N and Fe and the consequences for the oxygen reduction reaction in acid medium has been studied. For this, a series of multiwalled carbon nanotubes with mean diameters of 10, 20 and 60 nm have been thermally treated in acid media and modified by addition of N- and Fe-groups by means of thermal treatments under inert atmosphere. The chemically treated nanotubes and the FeN-CNTs have been thoroughly characterized by N_2 adsorption/desorption isotherms, Raman spectroscopy, X-ray photoelectron spectroscopy, elemental analysis, thermogravimetric analysis and X-ray diffraction. The performance of the FeN-CNTs for the oxygen reduction reaction (ORR) in acid medium has been evaluated by means of electrochemical techniques. We have found that the amount of nitrogen actually incorporated onto the multiwalled carbon nanotubes, which ranges between 2 and 3 wt.%, can be directly related with the number of defects of the chemically treated multiwalled nanotubes. On the other hand, the BET specific surface area of the FeN-CNTs increases with the decreasing diameter of the CNTs. A direct relationship between the nitrogen external surface area and the ORR performance has been observed.

1. Introduction

Proton exchange membrane fuel cells (PEMFCs) are very efficient devices for the conversion of the energy storage in molecules such as H_2 into electricity [1]. In particular, PEMFCs are expected to be widely implemented in the transportation sector and in portable devices because of their low operating temperature which enables

* Corresponding author. Tel./fax: +34 91 585 4632.
** Corresponding author. Tel.: +966 541 886660.
E-mail addresses: masalam16@hotmail.com (M.A. Salam), srojas@icp.csic.es (S. Rojas).

0378-7753/$ – see front matter © 2013 Elsevier B.V. All rights reserved.
http://dx.doi.org/10.1016/j.jpowsour.2013.04.086

fast start-up and because of their high power densities of 0.9 W cm^{-2} at 0.60 V cell voltage which meets automotive packaging requirements. However, the current price per kW ($61 kW^{-1} in 2009) for PEMFCs still doubles the price target of $30 kW^{-1} by 2015 of the US Department of Energy (DOE) for PEMFCs to become a competitive technology against internal combustion engines [2].

The low efficiency of Pt/C electrocatalysts for the oxygen reduction reaction (ORR) is amongst the most significant obstacles preventing the widespread utilization of PEMFCs. At the practical level, this issue must be compensated either by using higher Pt loadings on the cathode electrode resulting in very high prices per kW or by designing bimetallic M–Pt-based catalysts [3]. However, large-scale applications would only be possible if non-expensive technologies are available. Moreover, features such as noble metal scarcity and Pt degradation in the cathode must be also considered for the designing of efficient ORR electrocatalysts.

In this sense, non-precious metal catalysts (NPMCs) are strong candidates for replacing Pt in the cathode of PEMFCs. This is because they are less expensive and more abundant than noble metals [4] and their lower kinetics for the ORR as compared to Pt electrodes, can be compensated by using higher amounts of catalysts without severe economic repercussions.

Since 1964, when Jasinski observed that cobalt phthalocyanine catalyzed the ORR [5], a number of approaches have been explored to design very active NPMCs for the ORR. Most works on non-precious metal oxygen reduction catalysts deal with nitrogen-coordinated iron or cobalt moieties within a carbon matrix, usually referred to as Fe/N/C or Co/N/C [4,6,7]. Graphene-coordinated FeN_4 or FeN_{2+2} and CoN_4 or CoN_2 moieties have been proposed as the actual active sites in NPMCs [8–11]; however, their actual nature remains mostly elusive hitherto. In this line, some recent studies unveil the importance of the protonation of the FeN_x and/or of the vicinal N_x sites for the ORR [12]. However, it has been also reported that the loss the performance of PEM fuel cells with Fe/N/C cathodes decreases due to the protonation of pyridinic nitrogen [13].

When it comes to the synthesis of the NPMCs conflicting results have been also reported. On the one hand, it has been observed that rather different synthetic routes lead to catalytic systems with virtually identical catalytic properties suggesting that different types of active sites endowed with similar catalytic performances can exist [4]. On the other hand, the relevance of features such as the nature of the carbon, nitrogen and Fe (or Co) sources, the thermal treatment and the presence of (bi)sulphate anions or other sulphur species are recognized to play a chief role in the final morphology and catalytic performance of NPMCs for the ORR. The exact relevance of the aforementioned features is not fully understood and it seems to depend on the catalytic precursors; however, certain tendencies are well documented. For instance, in order to achieve highly active electrocatalysts thermal treatments in the presence of N and Fe sources above 600 °C are needed. The kinetics of these Fe/N/C electrodes is around 150–200 mV below that of Pt/C. In part, this is because Fe/N/C and Co/N/C electrocatalysts have a lower number of active sites per unit volume than Pt/C electrocatalysts. Higher activities have been reported by optimizing the thermal treatment and/or by using aniline as the source of N and carbon. As for the first approach, it has been reported that thermal treatment of amorphous carbons in NH_3 atmosphere at around 950 °C leads to the creation of a high number of N-containing micropores and as a result to a higher amount of active sites leading to ORR kinetics activity as high as 98 A cm^{-3} [4,14–17]. A remarkably enhance of the catalytic performance of NPMCs for the ORR has been achieved by using nitrogen–carbon composites, in particular by using polyaniline as precursor to a carbon–nitrogen template ORR overpotentials within mere ~60 mV away of the state-of-the-art of carbon-supported platinum electrocatalysts [7,18] have been reported.

Although Fe/N/C and Co/N/C electrocatalysts have shown promising activities towards the ORR, more research efforts are needed in order to fully understand features such as the real structure of the active sites, mass transport effects and to increasing the long-term stability of Fe/N/C and Co/N/C based electrocatalysts in acid environments.

There is a wide consensus in that the durability of NPMCs increases with the increasing graphitization degree of the carbon support [4,19]. It has been reported that MWCNTs lead to more resistance catalysts than carbon blacks despite of their lower initial activity [20]. In this line, nitrogen-doped carbon nanotubes display promising performances in the ORR in terms of both activity and durability [21–26]. Furthermore, higher stability and higher ORR activities with N-doped carbon nanotubes supported Fe have been reported [27]. In order to increase the ORR activity of NPMCs based on carbon nanotubes it is necessary to understand the features that control the incorporation of Fe and N onto the graphitic structure of the nanotubes. The present study explores the effects of the radii of commercial multiwalled carbon nanotubes (CNTs), for the synthesis of FeN-CNTs electrocatalysts, and the repercussions in their performance for the oxygen reduction reaction.

2. Experimental

2.1. Synthesis of FeN-CNTs

Three set of commercial multiwalled carbon nanotubes (CNTs) with different diameters of 10, 20 and 60 nm were obtained from Shenzhen Nanotech Port Co., Ltd (China) have been modified by creating Fe/N_x groups within their structures. Initially, the CNTs were functionalised in a sulfonitric mixture of 5.5 M H_2SO_4/3.0 M HNO_3 during 2 h at 333 K. The functionalized CNTs were labelled as t-CNT60, t-CNT20 and t-CNT10 (generally referred to as t-CNTs) after the average diameter of the nanotubes of 10, 20 and 60 nm, respectively. Then a N-rich polymeric resin (urea-formaldehyde) was deposited on t-CNTs by following a previously reported approach [24]. Briefly, carbon and urea were mixed with formaldehyde (molar ratio 1:2) in deionized water under stirring. When the temperature of the solution reached 323 K, the required volume of 1 M NaOH solution to adjust the pH to 10.0 was added. The polymerization reaction was initiated by increasing the reaction temperature to 347 K and the condensation reaction was triggered by acidifying the solution to pH 2.5 with a 0.5 M H_2SO_4 solution while stirring. The stirring was kept for 1 h and the resulting gel was dried overnight at 353 K. The obtained samples are referred to as N-CNTs. Then, the deposition of Fe–ethylenediamine complex on the N-CNTs was performed. The necessary amount of $FeSO_4 \cdot 7H_20$ to obtaining a theoretical Fe concentration of 12 wt.% in the final catalyst was added to an ethanol solution containing ethylenediamine. The N-CNTs prepared previously were dispersed into the Fe-containing solution and refluxed at 80 °C for 3 h. Finally, the liquid phase was removed in a rotatory evaporator under vacuum. The resulting solid was thermally treated in N_2 atmosphere (pyrolyzed) at 1073 K during 1 h. Finally, the pyrolyzed sample was treated in 0.5 M H_2SO_4 at 333 K in order to remove non-stable acid-soluble Fe–N phases. The Fe/N modified t-CNTs obtained after the pyrolysis steps are labelled as FeN-CNT60, FeN-CNT20 and FeN-CNT10.

2.2. Structural characterization

X-ray diffractograms were collected on a Seifert 3000 powder diffractometer operating with Cu Kα radiation (λ = 0.15418 nm)

generated at 40 kV and 40 mA. Scans were recorded at 0.02° s^{-1} for 2θ values between 10° and 90°.

X-ray photoelectron spectra (XPS) of the samples were acquired with a VG Escalab 200R spectrometer fitted with a Mg Kα ($h\upsilon$ = 1253.6 eV) 120 W X-ray source. The energy regions of the photoelectrons of interest were scanned until an acceptable signal-to-noise ratio was achieved. Intensities were estimated by calculating the integral of each peak, determined by subtraction of the Shirley-type background and fitting of the experimental curve to a combination of Lorentzian and Gaussian lines of variable proportions. Accurate binding energies (±0.2 eV) were determined by referencing to the C 1s peak at 284.6 eV.

Carbon, nitrogen and hydrogen contents of the samples were measured with an elemental analyser (LECO CHNS-932).

Raman spectra of different samples were recorded in air using a single monochromator Renishaw system 1000 equipped with a thermoelectrically cooled CCD detector and holographic super-Notch filter. The samples were excited with the 535 nm Ar line. The instrument is internally calibrated with a silicon reference at 520 cm^{-1} and gives a peak position resolution of 1 cm^{-1}, the spectrum acquisition time was 10 s and 10 spectra were acquired to ensure an optimal signal-to-noise ratio.

Textural properties were evaluated by N_2 adsorption–desorption isotherms of the samples recorded at liquid N_2 temperature with a Micromeritics ASAP 2000 apparatus. Samples were degassed at 150 °C under vacuum for 24 h. Specific areas were calculated by applying the BET method within the relative pressure range P/P^0 = 0.05–0.30.

Transmissions Electron Microscopy (TEM) studies of the samples were made with a JEOL JEM 2100FX microscope operating at 200 keV, point resolution of 0.31 nm. The specimens for analysis were prepared by dispersing the powdered sample in ethanol using an ultrasonic bath. A drop of each resulting suspension was placed on a copper grid covered with a porous carbon film. Energy Dispersive X-ray Spectrometer (EDS) analysis was performed with an INCA (Oxford Instruments Ltd.) detector and an INCAEnergy software package.

2.3. Electrochemical characterization

The electrochemical experiments were performed by using a computer controlled Autolab Pgstat 302N potentiostat/galvanostat.

A standard three-compartment glass cell and a rotating disk electrode (RDE) (Pine research Instruments) were used for all electrochemical experiments. The counter electrode was a graphite rod and the reference electrode was an Ag/AgCl electrode (Methrom Switzerland). In this manuscript potentials are quoted with respect to the RHE.

A glassy carbon electrode with a thin film of the electrocatalyst under study was used as the working electrode. For the thin film preparation, samples were dispersed ultrasonically for 10 min in a mixture of Millipore Milli Q® water, isopropyl alcohol (Aldrich, 99.8%) and Nafion (5 wt.%) with a final ratio of 80 vol%, 18.8 vol% and 0.2 vol%, respectively. The final concentration of the electrocatalyst in the suspension was 6 $mg_{cat}\ L^{-1}$. A volume of 20 μL of the suspension was pipetted onto the previously polished glassy carbon tip of the RDE.

Previous to the electrochemical testing, the working electrode was electrochemically cleaned by potential cycling from 0 to 1.1 V *vs.* RHE for 50 cycles in Ar-saturated 0.1 M $HClO_4$ electrolyte. Cyclic voltammograms were recorded between 0 and 1.0 V at 10 mV s^{-1} in N_2-saturated 0.1 M $HClO_4$.

ORR polarization curves were collected by means of the RDE technique between 0 V and 1 V at 10 mV s^{-1} and 1600 rpm in O_2-saturated 0.1 M $HClO_4$ electrolyte. The Faradaic current density (J_F mA cm^{-2}) was obtained by subtracting the current obtained during the anodic sweep scan in the O_2-saturated electrolyte from the capacitive current obtained in the potential sweep recorded in Ar-saturated O_2-free electrolyte under the same experimental conditions. The ORR kinetic current (I_k) was calculated by using the relationship between I_k and I_F as established by the Koutecky–Levich equation ($I_k = -I_F \cdot I_{lim}/(I_F - I_{lim})$) where I_K is the kinetic current density defined as <0 for reduction reactions and I_{lim} is the limiting current density. Finally, the ORR mass activity is defined by $I_M = -I_K/m_{cat}$ where m_{cat} is the catalyst loading expressed in g cm^{-2} [6].

3. Results and discussion

The composition of the FeN-CNTs, more specifically the H, C and N contents, have been determined by elemental analysis and are reported in Table 1. The amounts of nitrogen incorporated into the CNTs range between 2.9 and 2.2 wt.%, in line with the contents reported for other CNT-based NPMCs [27]. Usually, a direct correlation between the nitrogen content and the ORR activity has been reported [28,29]; however, this correlation has been convincingly questioned by the same group arguing that the actual factor controlling the kinetics of the ORR is the amount of micropores created during the thermal treatment of the samples [16]. As deduced from the data reported in Table 1, the catalyst prepared with the nanotubes with the smaller diameter, FeN-CNT10 is the one containing the lower amount of nitrogen and as a consequence the one whit the lower N/C ratio. However, a close inspection of Table 1 reveals that the actual amount of nitrogen incorporated onto the FeN-CNT does not follow a straight correlation with the diameter of the FeN-CNTs and that the catalyst having the higher amount of nitrogen is FeN-CNT20.

The Fe 2p, C 1s, N 1s and O 1s core-level spectra of the FeN-CNTs were recorded in order to estimate the relative surface abundance of the elements and to identify the different N, C and Fe species in the samples. The N 1s core-level spectra of FeN-CNT60, FeN-CNT20 and FeN-CNT10 are shown in Fig. 1. The N 1s spectra have been fitted to three components with peak maxima at 398.5, 400.1 and 401–401.5 eV, and assigned to pyridinic-N, pyrrolic-N and graphitic-N species, respectively [6,24]. As shown in Table 1, the

Table 1
C, H, N contents and N/C bulk content from elemental analyses and N/C, Fe/C and O/C surface atomic ratios derived from XPS FeN-CNT60, FeN-CNT20, FeN-CNT10 and of the parent t-CNTs.

Sample	C, H and N content (wt.%)				Surface atomic content (XPS)			Relative atomic amount of N species		
	C	H	N	N/C	N/C	O/C	Fe/C	Pyridinic N	Pyrrolic N	Graphitic N
FeN-CNT60	81.3	0.8	2.6	0.033	0.040	0.11	–	0.36	0.22	0.42
FeN-CNT20	82.7	1.2	2.9	0.035	0.036	0.06	0.004	0.40	0.33	0.27
FeN-CNT10	80.0	1.2	2.2	0.027	0.022	0.08	–	0.28	0.31	0.41
t-CNT60	96.1	0.1	0.1	–	–	0.05	–	–	–	–
t-CNT20	95.4	0.2	0.1	–	–	0.03	–	–	–	–
t-CNT10	92.1	0.2	0.1	–	–	0.03	–	–	–	–

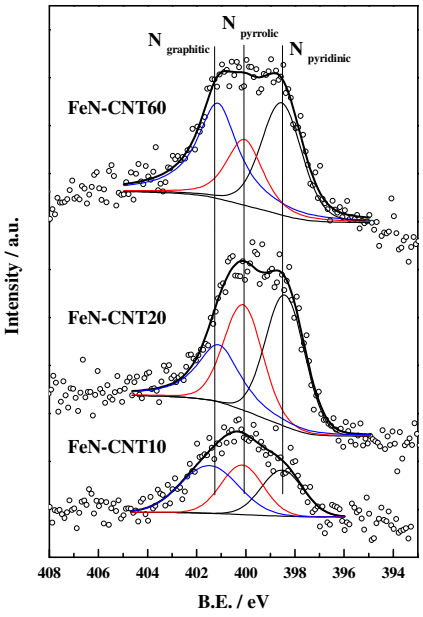

Fig. 1. XPS spectra of the N 1s core-level region of FeN-CNT10, FeN-CNT20 and FeN-CNT60. The contribution of N-graphitic, N-pyrrolic and N-pyridinic species to the total N 1s region is shown in each spectrum in blue, red and black lines, respectively. (For interpretation of the references to colour in this figure legend, the reader is referred to the web version of this article.)

surface atomic N_{at}/C_{at} ratio increases with nanotube diameter from 0.022 for FeN-CNT10 to 0.034 and 0.040 for FeN-CNT20 and FeN-CNT60, respectively (see Table 1). This trend is also observed if the N/C ratios obtained by the elemental analyses are considered. Thus, the N/C bulk ratios of the FeN-CNTs also increase with the nanotube diameter from 0.027 for FeN-CNT10 to 0.035 and 0.033 for FeN-CNT20 and FeN-CNT60, respectively. The fairly good coincidence between bulk and surface N/C ratios indicates that the majority of the N atoms created upon CNT modification are created on the surface of the nanotubes.

As stated above, three different N-containing species are detected by XPS analyses. Some works suggest that the pyridinic type of nitrogen lead to the most active sites for the ORR [28,30]; however a direct correlation between the type of nitrogen and the ORR performance remains elusive [6]. The relative amount of pyridinic-N, pyrrolic-N, and graphitic-N species is roughly similar in all of the FeN/CNT catalysts and only some marginal differences in their surface abundance can be observed (see Table 1). For instance, the relative amount of pyridinic nitrogen in FeN/CNT10 is the lowest in the series yet this is the most active catalyst for the ORR (see below).

According to these results, it can be concluded that the amount of nitrogen incorporated onto the nanotubes, more specifically, the N/C ratio, becomes influenced by the diameter of the chemically treated CNTs, and it increases with the increasing nanotubes' diameter. On the other hand, the nature of nitrogen species created onto the C-network of the nanotubes is not significantly influenced by the diameter of the CNTs and all FeN-CNTs display a quite similar type of relative proportion of N-species.

Fe/C surface atomic ratios have been measured by XPS and the values are reported in Table 1. Remarkably, the content of surface Fe species is very low, probably because they are below the detection limit of the XPS analysis, and FeN-CNT20 is the only sample showing the presence of surface Fe species. Given that XPS is a surface sensitive technique (the depth of the analysis being ca. 5–6 nm), and that the presence of iron has been detected by other characterization techniques such as XRD, the lack of observation of XPS peaks within the binding energy region of the Fe 2p photoelectrons suggests that Fe species are predominantly encapsulated within graphitic or amorphous carbon layers.

Fig. 2 shows the X-ray diffractograms of FeN-CNT60, FeN-CNT20 and FeN-CNT10 along with those of the t-CNTs. The first observation that should be noted is that the (002) stacking diffractions at $2\theta = 25^\circ$ of graphite are observed in all samples (see Fig. 2) indicating that the structure of the t-CNTs remains stable after the incorporation of both N and Fe groups.

The diffractograms of the Fe–N/CNTs electrocatalysts display a set of diffraction peaks indicative of the presence of the Fe_3O_4 phase. The presence of such Fe_3O_4 phase clearly indicates that addition of Fe to the N-modified t-CNTs does not lead to the exclusive formation of Fe/N_x moieties after the thermal treatments. Although the actual nature of the active site remains elusive, there is a strong consensus in that Fe/N_x moieties, probably as FeN_4 and/or FeN_{2+2} species, are the active sites for the ORR reaction [27,31]. In principle, Fe oxide phases should have been dissolved during the acid leaching treatment so it would be reasonable to assume that the Fe_3O_4 species detected by XRD, by being encapsulated within the CNTs, are not responsible of the ORR activity.

Finally, weak reflections ascribed to the presence cobalt and/or nickel metallic phases are observed in all of the diffractograms and ascribed to metal impurities probably remaining from nanotubes synthesis. This observation is in good agreement with SEM and EDX analyses (not shown) that also confirmed the presence of Co in t-CNT10 and FeN-CNT10 and of Ni in t-CNT20 and t-CNT60 and FeN-CNT20 and FeN-CNT60. As shown below, these impurities have no effects in the catalytic performances of the FeN-CNTs for the ORR.

Fig. 3 depicts the first order Raman spectra of FeN-CNT60, FeN-CNT20 and FeN-CNT10 and of the parent carbon nanotubes, *i.e.* t-CNT60, t-CNT20 and t-CNT10, respectively. In general, the Raman spectrum of graphitic materials shows two bands at 1580 cm^{-1} and 1351 cm^{-1}, usually referred to as G band and D band, respectively [32,33]. The D band, which requires one phonon and one defect be activated [34], accounts to the discontinuity of the graphite planes at the edges [33]. In this sense, the crystallinity or "perfection" of graphitic structures can be established from the relative intensity of D and G bands (I_D/I_G). Table 2 summarizes I_D/I_G values of the different samples studied.

As shown in Fig. 3, the I_D/I_G ratio is characteristic of each t-CNT and although it remains roughly constant after the incorporation of the nitrogen and Fe groups a slight increasing for FeN-CNT10 and

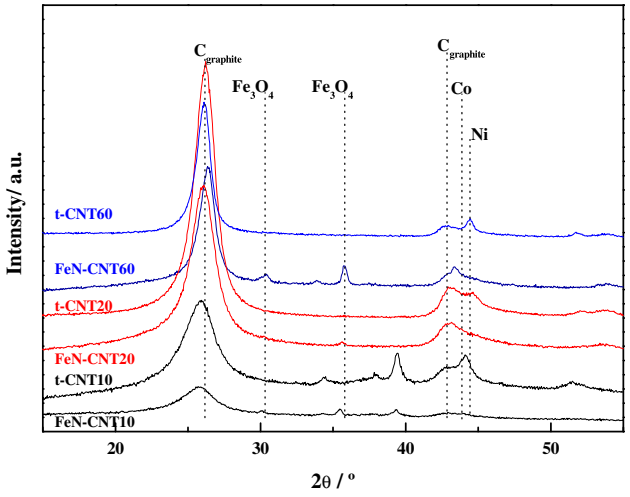

Fig. 2. X-ray diffractograms of the functionalized t-CNTS and of the FeN-CNTs. Diffraction lines due to the presence of Fe_3O_4, Co and Ni are observed.

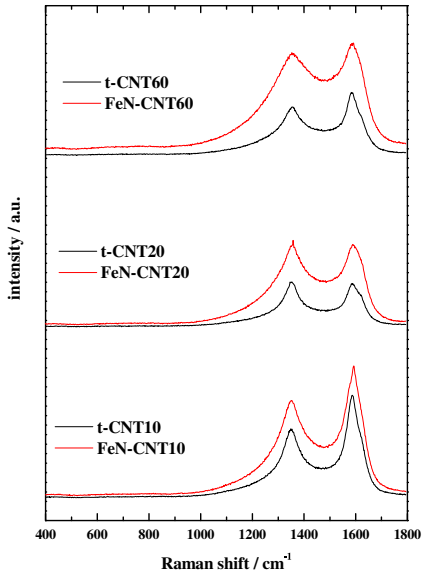

Fig. 3. Raman spectra of the functionalized t-CNTs (black line) and of the FeN-CNTs (red line). (For interpretation of the references to colour in this figure legend, the reader is referred to the web version of this article.)

FeN-CNT60 samples is observed. However, the profile of the D bands of the FeN/CNTs is much broader than that of the D bands of the corresponding t-CNTs. The broadening of the D bands suggests that the incorporation of the N and Fe groups increases the structural imperfection of the sp^2 network [32].

The I_D/I_G ratio increases in the sequence FeN-CNT10 < FeN-CNT60 < FeN-CNT20 and as a consequence the amount of edged planes follows the same trend [33]; *i.e.* FeN-CNT20 > FeN-CNT60 > FeN-CNT10. It has been recently reported that the exposure of edged planes facilitates the incorporation of nitrogen to carbon structures [24], and the results obtained in our work goes in line with this observation. Thus, the sample with the highest exposure of edge planes, FeN-CNT20, is the sample containing the highest amount of nitrogen as determined by elemental analysis. The direct relationship between nitrogen incorporated onto the nanotubes and the I_D/I_G ratio of the nanotubes also applies to FeN-CNT60 and FeN-CNT10. Furthermore, the surface N_{at}/C_{at} ratios derived from the XPS also follow a similar trend; FeN-CNT20 ≈ FeN-CNT60 > FeN-CNT10, only in this case the surface N_{at}/C_{at} ratio of FeN-CNT60 is slightly higher than that of FeN-CNT20 as shown in Table 1.

Table 2 shows the BET surface area, micropore area and external surface area values of all samples studied. The BET surface area value of the samples increases after the incorporation of N and Fe onto the t-CNTs. The BET area increase of FeN-CNT60 and FeN-CNT20 is of ca. two fold with respect to the BET areas of t-CNT60 and t-CNT20. The increasing of the BET area accounts to the increasing of the micropore surface area during the synthesis of the F/N/CNTs catalysts. By contrast, the micropore area of t-CNT10 is not modified during the synthesis of FeN-CNT10 and as a consequence its BET area is only ca. 25% higher than that of CNT10. This result could indicate that the degree of graphitization of the CNT10 nanotubes is higher than that of CNT20 and CNT60 and therefore it is more stable under the thermal treatment in N_2 atmosphere.

Table 2
BET, external and micropore surface areas of the FeN-CNTs electrocatalysts and of t-CNTs. The last column is the ratio of first order D and G Raman bands.

Sample	BET surface area/$m^2\ g^{-1}$	External surface area/$m^2\ g^{-1}$	Micropore surface area/$m^2\ g^{-1}$	I_D/I_G
FeN-CNT60	112	69	43	0.91
FeN-CNT20	252	160	92	1.03
FeN-CNT10	306	303	3	0.78
CNT60	61	58	3	0.81
CNT20	131	124	7	1.03
CNT10	258	251	7	0.72

Fig. 4 shows TEM images of the functionalized nanotubes (t-CNT) and of the Fe-CNTs. Clearly, the diameter of the nanotubes increases in the order CNT10 < CNT20 < CNT60. It can be also observed how the structure of the nanotubes is preserved after the incorporation of Fe/N moieties onto the nanotubes. The presence of Fe has been identified in all FeN-CNTs by means of EDS analyses (not shown). However, in good agreement with XRD analysis, Fe clusters have been observed by TEM only in FeN-CNT60. This result suggests that the active centres for the ORR are formed by monoatomic Fe/N sites rather than by clusters of Fe oxide or carbide species.

Fig. 5 shows the cyclic voltammograms of the FeN-CNTs electrocatalysts recorded at 10 mV s^{-1} in Ar-saturated 0.1 M $HClO_4$. The shape of the voltammograms is similar in all cases showing a square wave profile typical of potential-independent capacitive response [6]. The capacitive current increases with the surface area of samples; however, the differences of the capacitive currents between the FeN-CNTs and the t-CNTs cannot be ascribed only to their higher surface area. Notwithstanding its lower surface area, FeN-CNT60 records higher capacitive currents than CNT10. This observation clearly illustrates that capacitive currents might account also to the contribution of a pseudo-capacitance response of redox sites. Thus, the higher capacitive current of the FeN-CNTs could be ascribed to a series of redox processes involving the surface functional groups created during the incorporation of the Fe/N groups or even to the iron containing species.

Fig. 6 shows the ORR polarization curves of the different electrocatalysts after subtraction of their corresponding capacitive current. First of all, it is worth to indicate that the FeN-CNTs samples show greater current densities than the non-modified t-CNTs. This feature indicates that the activity towards the ORR of the Ni and Co phases remaining on the t-CNTs is negligible as compared to that of the Fe/N_x centres created during the synthesis of the electrocatalysts. Remarkably, the activity of the FeN-CNTs samples for the ORR decreases with the increasing diameter of the t-CNTs used for their synthesis. In this sense, a careful comparison between Figs. 5 and 6 shows that the samples recording the highest capacitive currents (Fig. 5) also show the higher ORR activity (Fig. 6).

The ORR kinetic data for the FeN-CNTs obtained from the Tafel plots of electrode potential versus kinetic (mass transport corrected) current densities are collated in Table 3. As observed the onset potential for the ORR lays between 0.84 V for FeN-CNT10 and 0.77 V for Fe-CNT60. Also, the exchange current density for the FeN-CNT10 (2.1×10^{-8} A cm^{-2}) is the highest in the series, being one order of magnitude higher than that measured with FeN-CNT60. The highest i_0 value reported to date for NPMCs is of 4×10^{-8} A cm^{-2}, as reported for PANI-Fe–C catalyst [7]. Two Tafel slope values of 60 and 120 mV dec^{-1} for the ORR on Pt at potentials higher and lower than 0.8 V are usually reported. The Tafel slope values of the FeN-CNTs lay between 101 and 108 mV dec^{-1}. Such high Tafel slope values are indicative of complicated ORR mechanism indicating that the ORR mechanism in the FeN-CNTs involves both the migration of intermediates and electron transfer processes [7].

Fig. 7 shows the mass activities of the FeN-CNTs electrocatalysts in the kinetically controlled potential region. The performance of FeN-CNT10 is superior to that of FeN-CNT20 and FeN-CNT60 throughout the whole polarization range. The mass activity of the catalysts at 0.8 V is shown in Fig. 8. Clearly, FeN-CNT10 exhibits the highest mass activity in the series, reaching a value of ~0.37 A g^{-1}

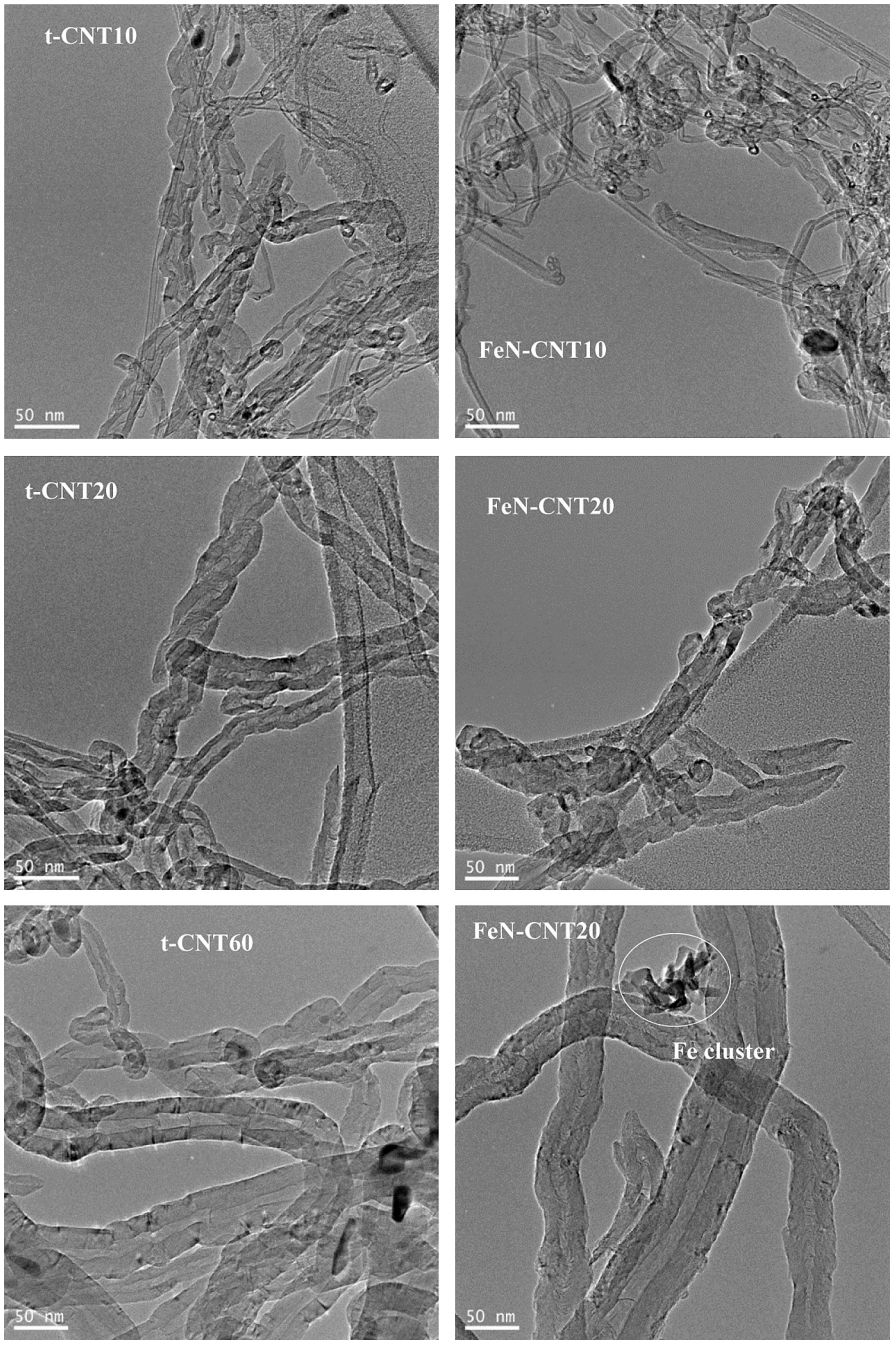

Fig. 4. TEM micrographs of the fresh nanotubes and of the FeN-CNTs. The presence of Fe clusters in FeN-CNT60 is indicated in the figure.

at 0.8 V, a current density value that compares well against those reported for other FeN-modified CNTs [27]. A direct correlation between the diameter of the nanotubes and the catalytic activity of the FeN/CNT samples in the ORR is observed in Fig. 6. The question arises as to how the diameter of the nanotubes can influence the kinetics of the FeN/CNT catalysts for the ORR. In principle, higher ORR activities are due to either (or both) a higher amount of active sites or/and to a higher intrinsic activity of those sites, *i.e.* higher turnover frequency (TOF). However, quantifying the number of active sites is not an easy task for Fe/N/C catalysts. Firstly, the actual nature of the sites remains mostly unknown and some studies even suggest that the ORR activity is not influenced by the presence of Fe, but it correlates well with the presence of nitrogen [22] either as pyridinic-N [25] and/or graphitic-N [24]. Nevertheless, most studies coincide in that FeN_4 and FeN_{2+2} ensembles are active sites of Fe/N/C electrocatalysts for the ORR [4], but it is also admitted that a significant fraction of the nitrogen and Fe atoms incorporated into Fe/N/C electrocatalysts do not form part of the sites. Therefore, the correlation between surface Fe concentration of N-coordinated Fe and the catalytic activity in the ORR is usually reported [27]. In the following we will try to unveil if such correlation exists for the Fe/N/C catalysts.

As shown above, the nitrogen content of the FeN-CNTs ranges between ca. 2 and 3 at.%, as deduced from elemental analyses. The ability of the carbon nanotubes for incorporating nitrogen goes in parallel with their structural imperfection (related to the ratios of the D and G bands in the Raman spectra) and follows the order: FeN-CNT20 > FeN-CNT60 > FeN-CNT10. On the other hand, XPS

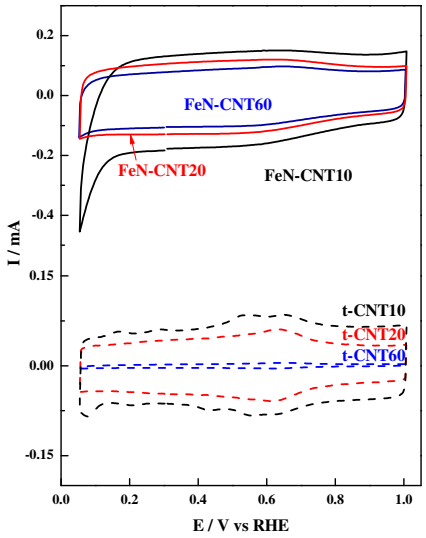

Fig. 5. Cyclic voltammograms of the functionalized t-CNTs (dot lines) and of the FeN-CNTs electrocatalysts in 0.1 M $HClO_4$ at 10 mV s^{-1}. Sample loading 0.6 mg cm^{-2}.

clearly shows that nitrogen incorporation to the t-CNTs leads to three types of different N-species and that the majority of the nitrogen atoms are located on the surface of the FeN/CNTs. Since FeN-CNTs have roughly similar ratios of pyridinic-N and graphitic-N, the different performances in the ORR should be ascribed to different amounts of total nitrogen within the active sites rather than to an individual N-containing species. Interestingly, even though the incorporation of Fe into N-modified nanotubes is expected to be favoured by the presence of nitrogen atoms [11] the presence of Fe is not observed by XPS suggesting that the Fe atoms are covered by a graphitic carbon layer. It should be noted that Fe contents as low as 0.02 wt.% have been reported to increase ORR activity [35].

The results above show that FeN-CNT10 is the more active sample in the series for the ORR despite FeN-CNT20 and FeN-CNT60 have higher amounts of nitrogen and higher surface (N_{at}/C_{at}) and bulk N/C ratios. Altogether, these observations indicate that

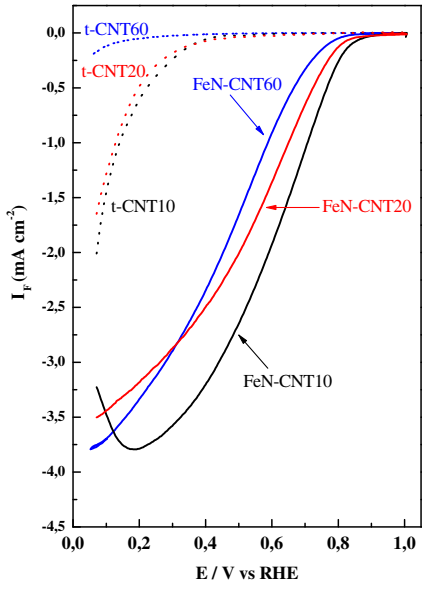

Fig. 6. Faradaic current (I_F) of the functionalized t-CNTs and of FeN-CNTs recorded during the positive going sweep in oxygen saturated 0.1 M $HClO_4$ at 10 mV s^{-1}, 1600 rpm. Sample loading 0.6 mg cm^{-2}.

Table 3
ORR kinetic data for FeN-CNTs obtained in O_2-saturated 0.1 M $HClO_4$ at 1600 rpm and 10 mV s^{-1}.

Catalyst	ORR onset/V[a]	$E_{1/2}$/V	Tafel slope/mV dec^{-1}	i_0/A cm^{-2}
FeN-CNT10	0.84	0.61	105	2.1×10^{-8}
FeN-CNT20	0.80	0.52	108	1.3×10^{-8}
FeN-CNT60	0.77	0.47	101	2.6×10^{-9}

[a] The onset potential has been defined as the potential at which a current density of 0.1 A cm^{-2} is generated [7].

the ORR activity follows a direct relation with the diameter of the carbon nanotubes but that the relationship between the nitrogen content and the activity is not so obvious.

In order to fully understand the activity of the FeN-CNTs samples in the ORR, the relevance of the external surface area of the FeN-CNTs (obtained by subtraction of the micropore area to the BET area, see Table 2) should be taken into account. Recent works have suggested that the active centres in the ORR are located within micropores created upon thermal treatment in NH_3 atmospheres of Fe- and N-containing carbon supports at controlled temperature and time [14,15]. However this line of reasoning cannot be translated to the FeN-CNTs reported in this manuscript since their microporosity is marginal as compared with their total area values. As a consequence we propose that the active centres of the FeN-CNTs should be located on the external surface of the nanotubes. With the idea in mind that the activity for the ORR should be correlated with the amount of exposed nitrogen, we have defined the nitrogen external surface area as the value of the external area multiplied by the amount of nitrogen in the sample as deduced by elemental analysis.

Fig. 9 shows the correlation between the mass activities (A g^{-1}) of the FeN-CNTs and their nitrogen external surface area (m^2_N g^{-1}). It can be observed how both parameters follow the same trend. Thus, FeN-CNT10 records the highest activity in the series followed by FeN-CNT20 and FeN-CNT60. The variation of the nitrogen external surface area follows exactly the same trend, and it decreases in the other FeN-CNT10 > FeN-CNT20 > FeN-CNT60. Remarkably, not only both mass activity and nitrogen external surface area follow the same trend, but more importantly, the magnitude of change in mass activity and in nitrogen external

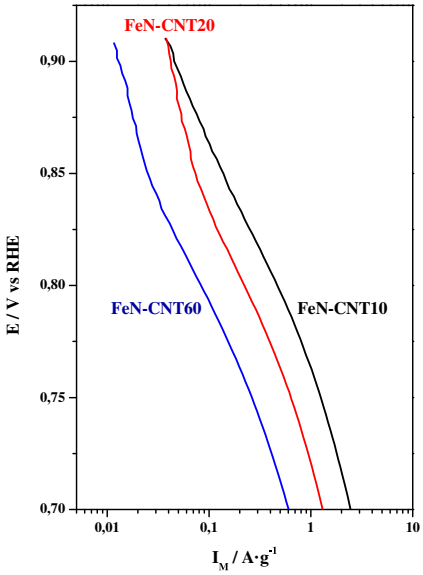

Fig. 7. Mass activities (I_M) of the FeN-CNTs measured in oxygen saturated 0.1 M $HClO_4$ at 10 mV s^{-1} and 1600 rpm. Catalyst loading 0.6 mg cm^{-2}.

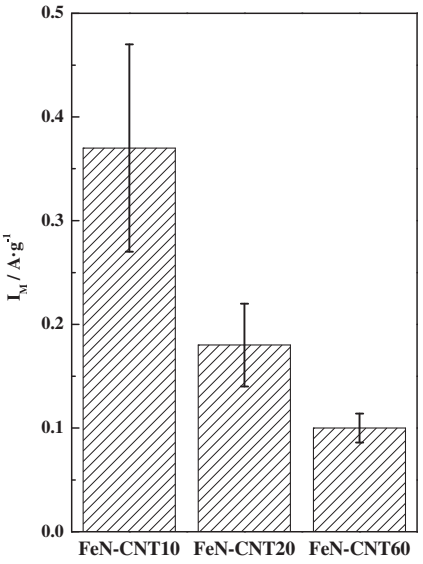

Fig. 8. Comparison of the ORR mass activities (I_M) of the Fe-CNTs electrocatalysts measured at 0.8 V. Error bars correspond to the standard deviation of three measurements. Oxygen saturated 0.1 M $HClO_4$ at 10 mV s^{-1} and 1600 rpm. Catalyst loading 0.6 mg cm^{-2}.

surface area is almost identical. These identical variations suggest that a direct relationship exists between the amounts of exposed N-containing sites and the ORR activity of FeN-CNTs.

In summary, our data suggests that the amount of nitrogen incorporated onto the nanotubes is not the most decisive parameter to define the ORR activity of FeN/CNT electrodes. Instead, the amount of exposed nitrogen, expressed as the nitrogen external surface area, is the fundamental parameter in determining the activity in the ORR. In order to improve the ORR activity of NPMCs based on Fe and carbon multiwalled nanotubes two features are necessary; (*i*) increasing the amount of N and Fe sites and, equally important (*ii*) increasing the exposure of the nitrogen sites. A strategy to fulfil both approaches would be to create a high number of defects into high area carbon nanotubes.

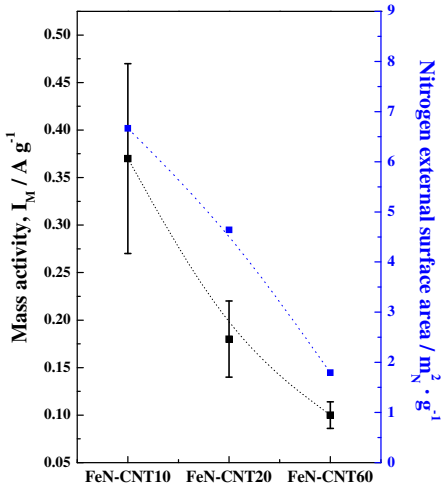

Fig. 9. Comparison of ORR mass activities at 0.8 V (black squares) and nitrogen external surface area (blue squares) points of all of the Fe-CNTs electrocatalysts. Error bars correspond to the standard deviation of three measurements. Oxygen saturated 0.1 M $HClO_4$ at 10 mV s^{-1}, 1600 rpm. Catalyst loading 0.6 mg cm^{-2}. (For interpretation of the references to colour in this figure legend, the reader is referred to the web version of this article.)

4. Conclusions

Multiwalled carbon nanotubes with different diameter, crystallinity and surface area have been modified by creating FeN ensembles within their structure by means of chemical addition of Fe- and N-containing precursors to the nanotubes and subsequent thermal treatment in nitrogen atmosphere. The amount of nitrogen incorporated onto the nanotubes is found to be dependent on the number of defects or graphitic edge of the nanotubes but the actual exposure of the nitrogen, defined by the external area of the different nanotubes, is the most important parameter for the ORR. Thus, the catalyst with the highest exposure of N, Fe-CNT10 reaches a mass activity of 0.73 A g^{-1} at 0.8 V, a value in line with the most active ones reported in literature for NPMCs with carbon nanotubes. The findings in this work suggest that the ORR performance of Fe/N/CNTs is controlled by both the amount of nitrogen incorporated and the fraction of nitrogen located within the external nanotube surface. Hence, increasing both parameters is the key to increasing the activity for the ORR of Fe/N/CNTs.

Acknowledgements

This project was funded by the Deanship of Scientific Research (DSR), King Abdulaziz University, Jeddah, under grant number (D-006-432). The authors, therefore, acknowledge with thanks DSR technical and financial support. Economic support from projects ENE2010-15381 from the Spanish Ministry of Science and Innovation and Project 201080E116 from the CSIC is also acknowledged.

References

[1] H.A. Gasteiger, S.S. Kocha, B. Sompalli, F.T. Wagner, Applied Catalysis B: Environmental 56 (2005) 9–35.
[2] Y. Wang, K.S. Chen, J. Mishler, S.C. Cho, X.C. Adroher, Applied Energy 88 (2011) 981–1007.
[3] I.E.L. Stephens, A.S. Bondarenko, U. Gronbjerg, J. Rossmeisl, I. Chorkendorff, Energy and Environmental Science 5 (2012) 6744–6762.
[4] F. Jaouen, E. Proietti, M. Lefèvre, R. Chenitz, J.P. Dodelet, G. Wu, H.T. Chung, C.M. Johnston, P. Zelenay, Energy and Environmental Science 4 (2011) 114–130.
[5] R. Jasinski, Nature 201 (1964) 1212–1213.
[6] F. Jaouen, J. Herranz, M. Lefèvre, J.P. Dodelet, U.I. Kramm, I. Herrmann, P. Bogdanoff, J. Maruyama, T. Nagaoka, A. Garsuch, J.R. Dahn, T. Olson, S. Pylypenko, P. Atanassov, E.A. Ustinov, ACS Applied Materials & Interfaces 1 (2009) 1623–1639.
[7] G. Wu, K.L. More, C.M. Johnston, P. Zelenay, Science 332 (2011) 443–447.
[8] A.L. Bouwkamp-Wijnoltz, W. Visscher, J.A.R. Van Veen, E. Boellaard, A.M. Van der Kraan, S.C. Tang, Journal of Physical Chemistry B 106 (2002) 12993–13001.
[9] M. Lefèvre, J.P. Dodelet, P. Bertrand, Journal of Physical Chemistry B 109 (2005) 16718–16724.
[10] U.I. Koslowski, I. Abs-Wurmbach, S. Fiechter, P. Bogdanoff, Journal of Physical Chemistry C 112 (2008) 15356–15366.
[11] A. Titov, P. Zapol, P. Král, D.-J. Liu, H. Iddir, K. Baishya, L.A. Curtiss, The Journal of Physical Chemistry C 113 (2009) 21629–21634.
[12] J. Herranz, F.d.r. Jaouen, M. Lefèvre, U.I. Kramm, E. Proietti, J.-P. Dodelet, P. Bogdanoff, S. Fiechter, I. Abs-Wurmbach, P. Bertrand, T.M. Arruda, S. Mukerjee, The Journal of Physical Chemistry C 115 (2011) 16087–16097.
[13] G. Liu, X. Li, P. Ganesan, B.N. Popov, Applied Catalysis B: Environmental 93 (2009) 156–165.
[14] M. Lefèvre, E. Proietti, F. Jaouen, J.P. Dodelet, Science 324 (2009) 71–74.
[15] E. Proietti, F. Jaouen, M. Lefèvre, N. Larouche, J. Tian, J. Herranz, J.P. Dodelet, Nature Communications 2 (2011).
[16] F. Jaouen, M. Lefèvre, J.-P. Dodelet, M. Cai, Journal of Physical Chemistry B 110 (2006) 5553–5558.
[17] M. Ferrandon, A.J. Kropf, D.J. Myers, K. Artyushkova, U. Kramm, P. Bogdanoff, G. Wu, C.M. Johnston, P. Zelenay, The Journal of Physical Chemistry C 116 (2012) 16001–16013.
[18] M. Lefevre, J.-P. Dodelet, ECS Transactions 45 (2012) 35–44.
[19] F. Charreteur, F. Jaouen, J.-P. Dodelet, Electrochimica Acta 54 (2009) 6622–6630.
[20] G. Wu, K. Artyushkova, M. Ferrandon, A.J. Kropf, D. Myers, P. Zelenay, ECS Transactions 25 (2009) 1299–1311.
[21] Z. Chen, D. Higgins, Z. Chen, Carbon 48 (2010) 3057–3065.
[22] Z. Chen, D. Higgins, H. Tao, R.S. Hsu, Z. Chen, The Journal of Physical Chemistry C 113 (2009) 21008–21013.

[23] Y. Ma, L. Sun, W. Huang, L. Zhang, J. Zhao, Q. Fan, W. Huang, The Journal of Physical Chemistry C 115 (2011) 24592–24597.
[24] H.S. Oh, J.G. Oh, W.H. Lee, H.J. Kim, H. Kim, International Journal of Hydrogen Energy 36 (2011) 8181–8186.
[25] C.V. Rao, C.R. Cabrera, Y. Ishikawa, The Journal of Physical Chemistry Letters 1 (2010) 2622–2627.
[26] K. Gong, F. Du, Z. Xia, M. Durstock, L. Dai, Science 323 (2009) 760–764.
[27] H.R. Byon, J. Suntivich, E.J. Crumlin, Y. Shao-Horn, Physical Chemistry Chemical Physics 13 (2011) 21437–21445.
[28] F. Jaouen, S. Marcotte, J.-P. Dodelet, G. Lindbergh, Journal of Physical Chemistry B 107 (2003) 1376–1386.
[29] D. Villers, X. Jacques-Bédard, J.-P. Dodelet, Journal of The Electrochemical Society 151 (2004) A1507–A1515.
[30] G. Faubert, R. Côté, J.P. Dodelet, M. Lefèvre, P. Bertrand, Electrochimica Acta 44 (1999) 2589–2603.
[31] J. Yang, D.-J. Liu, N.N. Kariuki, L.X. Chen, Chemical Communications (2008) 329–331.
[32] L.G. Bulusheva, A.V. Okotrub, I.A. Kinloch, I.P. Asanov, A.G. Kurenya, A.G. Kudashov, X. Chen, H. Song, Physica Status Solidi (B) Basic Research 245 (2008) 1971–1974.
[33] G. Compagnini, O. Puglisi, G. Foti, Carbon 35 (1997) 1793–1797.
[34] H. Wang, T. Maiyalagan, X. Wang, ACS Catalysis 2 (2012) 781–794.
[35] F. Jaouen, J.P. Dodelet, Electrochimica Acta 52 (2007) 5975–5984.